BIOCHEMISTRY

 Volume 44, Number 41 October 18, 2005

Articles

Molecular Dynamics Simulations of Salicylate Effects on the Micro- and Mesoscopic Properties of a Dipalmitoylphosphatidylcholine Bilayer†

Yuhua Song, Victor Guallar, and Nathan A. Baker*

Department of Biochemistry and Molecular Biophysics, Center for Computational Biology, Washington University, St. Louis, Missouri 63110

Received April 14, 2005; Revised Manuscript Received July 1, 2005

ABSTRACT: Salicylate, an amphiphilic molecule and a popular member of the nonsteroidal anti-inflammatory drug family, is known to affect hearing through reduction of the electromechanical coupling in the outer hair cells of the ear. This reduction of electromotility by salicylate has been widely studied, but the molecular mechanism of the phenomenon is still unknown. In this study, we investigated one aspect of salicylate's action, namely the perturbation of electrical and mechanical membrane properties by salicylate in the absence of cytoskeletal or membrane-bound motor proteins such as prestin. In particular, we simulated the interaction of salicylate with a dipalmitoylphosphatidylcholine (DPPC) bilayer via atomically detailed molecular dynamics simulations to observe the effect of salicylate on the microscopic and mesoscopic properties of the bilayer. The results demonstrate that salicylate interacts with the bilayer by associating at the water−DPPC interface in a nearly perpendicular orientation and penetrating more deeply into the bilayer than either sodium or chloride. This association has several affects on the membrane properties. First, binding of salicylate to the membrane displaces chloride from the bilayer−water interface. Second, salicylate influences the electrostatic potential and dielectric properties of the bilayer, with significant changes at the water−lipid bilayer interface. Third, salicylate association results in structural changes, including decreased headgroup area per lipid and increased lipid tail order. However, salicylate does not significantly alter the mechanical properties of the DPPC bilayer; bulk compressibility, area compressibility, and bending modulus were only perturbed by small, statistically insignificant amounts by the presence of salicylate. The observations from these simulations are in qualitative agreement with experimental data and support the conclusion that salicylate influences the electrical but not the mechanical properties of DPPC membranes.

Salicylate (2-hydroxybenzoic acid) is closely related to aspirin and is a member of the nonsteroidal anti-inflammatory family of drugs (*1*). Interestingly, salicylate has a number of hearing-related reversible side effects at high doses, including hearing loss, a decrease in spontaneous otoacoustic emissions, and tinnitus, all of which have been related, in part, to changes in the mechanical and electrical properties of the cochlear outer hair cell (OHC)[1] (*2*−*11*). OHCs play an important role in the sensitivity of mammalian hearing for high-frequency sounds through a mechanism of electromechanical feedback (*12*). While the exact molecular mech-

† This work was supported by NIH Grant R01 GM069702 (N.A.B. and Y.S.) and an Alfred P. Sloan Foundation Research Fellowship (N.A.B.).

* To whom correspondence should be addressed: Department of Biochemistry and Molecular Biophysics, Center for Computational Biology, Washington University, 700 S. Euclid Ave., Campus Box 8036, St. Louis, MO 63110. Phone: (314) 362-2040. Fax: (314) 362-0234. E-mail: baker@biochem.wustl.edu.

10.1021/bi0506829 CCC: $30.25
Published on Web 09/21/2005

Table 1: Salicylate and NaCl Concentrations for the Six Systems Simulated in This Study

system	[salicylate] (mM)	[NaCl] (mM)
pure DPPC	0	0
DPPC/10 mM SAL	10	0
DPPC/60 mM SAL	60	0
DPPC/NaCl	0	150
DPPC/10 mM SAL/NaCl	10	150
DPPC/60 mM SAL/NaCl	60	150

anism of salicylate's effect on OHC electromechanical response is still unknown, experimental work has suggested that salicylate may interact with several components of the OHC, including the phospholipid bilayer (*13*−*20*) and membrane-bound proteins such as prestin (*21*−*23*). In this study, we have investigated one aspect of salicylate's effects on OHC electromechanical coupling: the perturbation of electrical and mechanical biomembrane properties by salicylate in the absence of cytoskeletal components or membrane-bound motor proteins such as prestin. The goal of this study is to elucidate the atomic-scale influence of salicylate on the mesoscopic mechanical and electrical properties of a "model" dipalmitoylphosphatidylcholine (DPPC) membrane.

Molecular dynamics (MD) methods have proven to be a useful tool in studying several structural, energetic, and dynamic properties of lipid bilayers (*24*−*28*), as well as analyzing the interactions of various small molecules (*29*−*38*) and macromolecules (*39*−*42*) with biomembranes. This study leverages the tremendous effort that has gone into phospholipid force field development to use MD simulations to understand the effect of salicylate on the microscopic and mesoscopic properties of a model membrane.

MATERIALS AND METHODS

Molecular dynamics (MD) trajectories of the interaction of the salicylate with a DPPC bilayer were calculated with GROMACS version 3.2.1 (*43*). A total of six simulations were performed at varying salicylate and NaCl concentrations (see Table 1 and below). The following sections describe the methods used to set up and simulate each system.

Force Field Parameters and Starting Structures. The initial salicylate (SAL, 2-hydroxybenzoic acid; see Figure 1) structure was obtained from the HIC-Up database (*44*). This structure was transformed into a GROMACS united atom topology file using the PRODRG server (*45*). To obtain the all atom force field for the salicylate, nonpolar hydrogens were added manually and the steric, torsional, and angle parameters were assigned on the basis of the GROMACS force field in GROMACS version 3.2.1 (*43*). The atomic charges of salicylate were calculated from quantum mechanical/molecular mechanical (QM/MM) calculations. In these QM/MM calculations, we started from the minimized DPPC/10 mM SAL/NaCl system and selected a subsystem consisting of four salicylate molecules (in different conformations) and a solvation sphere of 1.6 nm around each of them (see

[1] Abbreviations: NpT, constant number−pressure−temperature; NVT, constant number−volume−temperature; DPPC, dipalmitoylphosphatidylcholine; GUV, giant unilamellar vesicle; HEK, human embryonic kidney; MD, molecular dynamics; OHC, outer hair cell; PME, particle-mesh Ewald; QM/MM, quantum mechanical/molecular mechanical; rms, root-mean-square; SAL, salicylate; SASA, solvent-accessible surface area; SOPC, stearoyloleoylphosphatidylcholine.

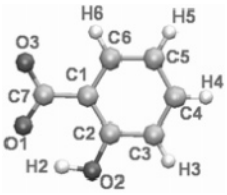

FIGURE 1: Salicylate, including the atom naming scheme used elsewhere in this paper.

Table 2: Salicylate Force Field Charge Parameters (in electron units)[a]

atom	charge (e)	atom	charge (e)	atom	charge (e)
O1	−0.843	C3	−0.307	H2	0.458
O2	−0.658	C4	−0.087	H3	0.167
O3	−0.731	C5	−0.237	H4	0.131
C1	−0.292	C6	−0.079	H5	0.131
C2	0.425	C7	0.803	H6	0.119

[a] See Figure 1 for the atom naming scheme.

Figure 1 of the Supporting Information). The system was further minimized using a QM/MM potential as implemented in QSite (*46*). The QM/MM methodology and protocol have been described extensively elsewhere (*47*, *48*). The quantum region consisted of the four salicylate molecules and all water molecules within 0.3 nm of them, for a total of 135 QM atoms. Geometry optimizations of salicylate were carried out using the B3LYP functional in combination with the 6-311G* basis set; the oxygen coordinates in the outermost 0.2 nm of solvation waters were held fixed. For the molecular mechanics potential energy function, QSite uses the OPLS-AA force field (*49*). The charges on the salicylate atoms were then obtained by fitting to the quantum electrostatic potential surface. The final charges used in the molecular dynamics simulation were obtained as the average of the four different salicylate units; these charges are listed in Table 2. While the differing local environments and conformations introduced small charge variations between the four salicylate molecules, adopting an (averaged) fixed charge parameter set for each salicylate was necessary for the long molecular dynamics runs. We are hopeful the advent of new efficient polarizable force fields (*50*) will obviate the need for fixed charges in future calculations.

The DPPC force field parameters used in this simulation were developed by Berger and Lindahl (*51*) and can be found in version 3.2.1 of GROMACS (*43*). These DPPC parameters have been shown to successfully reproduce experimental quantities such as lipid volume (*52*) and order parameters (*53*). The initial structure of a 64-lipid DPPC bilayer was obtained from the Tieleman group (*54*). A lipid bilayer composed of 256 DPPC lipids was generated by periodic replication of the 64-lipid Tieleman structure to give a system with lateral dimensions of roughly 10 nm × 10 nm. The choice of 256 DPPC lipids was a tradeoff between computational cost and the size of the system required to obtain reasonable continuum properties based on the previously published studies (*27*).

All the simulations were performed in a roughly 10 nm × 10 nm × 10 nm periodic box, thus ensuring more than 2 nm of solvent between the lipid surface and box boundaries to reduce potential artifacts arising from periodicity. This box was filled with 14422−15384 SPC (*55*) water molecules (depending on the system being simulated), corresponding

to a hydration level of 56−60 waters per lipid. The SPC water model was chosen on the basis of previous studies demonstrating its efficiency and relative accuracy for membrane simulations (*26*).

As mentioned above (see also Table 1), simulations were performed for six DPPC systems with different concentrations of salicylate and NaCl. The first system (pure DPPC) contained a DPPC bilayer and water only. The second (DPPC/10 mM SAL) contained four salicylates (corresponding to 10 mM salicylate) and four Na^+ ions (used to keep the system neutral). The third (DPPC/60 mM SAL) contained 20 salicylates (60 mM salicylates) and 20 Na^+ ions. The fourth (DPPC/NaCl) contained 50 Na^+ and 50 Cl^- ions (corresponding to 150 mM NaCl). The fifth (DPPC/10 mM SAL/NaCl) contained four salicylates, 54 Na^+ ions, and 50 Cl^- ions. The sixth (DPPC/60 mM SAL/NaCl) contained 20 salicylates, 70 Na^+ ions, and 50 Cl^- ions. During the simulation system setup, the ions and salicylates were randomly distributed in the water with the constraint that the minimum solute−solute and solute−lipid distances were greater than 6 Å. This constraint was imposed to prevent artificial ion pairing in the initial stages of the simulation.

Simulations. All six simulations followed the same molecular dynamics protocol. First, steepest descent minimization and 20 ps of constant number−pressure−temperature (NpT) molecular dynamics were performed with mobile water molecules but with the lipid bilayer, salicylate, and ions restrained. This short water equilibration was carried out at 50 K with isotropic pressure scaling to 1 atm and time steps of 1 fs. Next, the system was warmed gradually via a series of 10 ps constant number−volume−temperature (NVT) MD simulations at 50, 100, 150, 200, 250, and 323 K with SHAKE constraints and 2 fs time steps. Because of the slow relaxation of lipid bilayer systems (*27*, *56*), an additional 5 ns NpT MD trajectory was performed to fully equilibrate the system. The production trajectory was obtained through 25 ns of NpT dynamics at 323 K and 1 atm. The final temperature of 323 K was chosen to ensure simulation of the membrane in the liquid crystalline phase (*57*). The Parrinello−Rahman pressure coupling algorithm (*58*) was used to isotropically scale the pressure with a time constant of 2 ps, while the temperature was controlled by the Nosé−Hoover temperature coupling algorithm (*59*) with a time constant of 0.5 ps. Finally, SHAKE constraints were used on all hydrogen−heavy atom bonds to permit a dynamics time step of 2 fs. Electrostatic interactions were calculated with the particle-mesh Ewald method (PME) (*60*), thus avoiding the artifacts caused by electrostatic cutoffs (*61*, *62*). Both the direct space PME cutoff the Lennard-Jones cutoffs were set at 1.0 nm.

The simulations were performed on a variety of dual-processor shared memory machines, including 2-CPU Intel Pentium 4 (with Intel compilers), 2-CPU AMD Opteron (with Portland Group compilers), 2-CPU Apple G5 (with GNU compilers), and 4-CPU Intel Itanium2 (with Intel compilers) computers. On average, 10 ns of simulation required roughly 2 weeks (wall clock) of run time for the Itanium2 and 4 weeks of run time for the other platforms.

RESULTS AND DISCUSSION

The following sections discuss the effects of salicylate on the mesoscopic (continuum) and microscopic (molecular and atomic) properties of the DPPC system. In addition to the quantities presented below, time courses of collective properties such as system area, volume, and potential energy are presented in Figures 2−4 of the Supporting Information. Given the relevance of salicylate's effect on OHC electromotility, we have focused the analysis of our MD simulations on membrane structural, electrical, and mechanical properties. Additional data on salicylate's effect on membrane dynamical properties are available as Supporting Information.

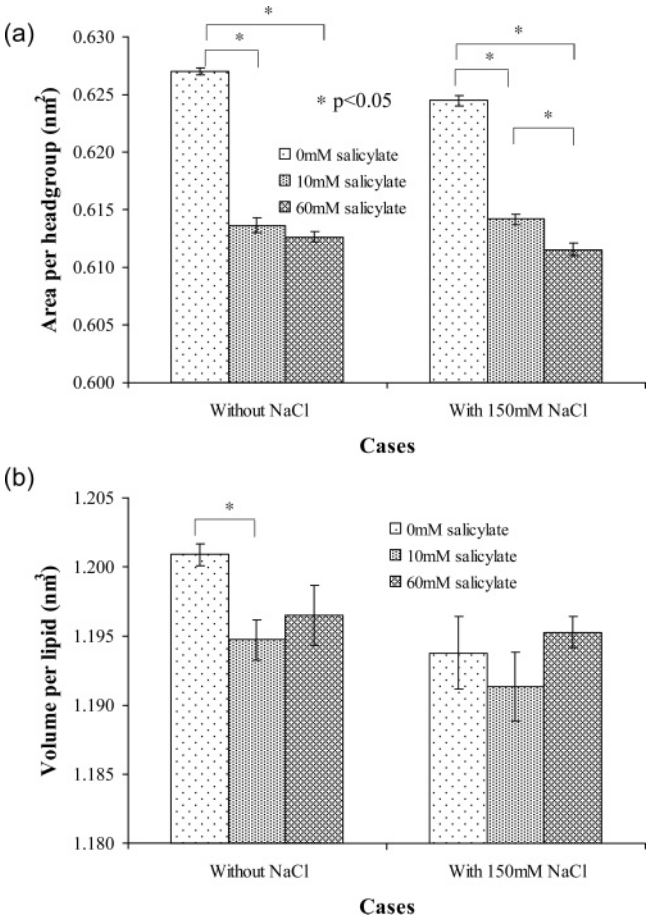

FIGURE 2: Effect of salicylate on (a) lipid headgroup areas and (b) per-lipid volumes. Error bars were calculated as described in the text.

Areas and Volumes. The headgroup or interfacial area per lipid molecule measures the average area occupied by each lipid in the bilayer (*63*). This quantity can be calculated from the projected area of the simulation box, i.e., the area spanned by the lateral dimensions of the system. The area per lipid headgroup is then the projected area divided by the number of lipid molecules. Using this definition, the average areas per lipid were calculated for the six systems and shown in Figure 2a with error bars obtained by the 5 ns block averaging scheme described above. The simulations produced an area per lipid for pure DPPC of 0.627 ± 0.001 nm^2, a value that is in reasonable agreement with the experimental result of 0.64 nm^2 (*64*). Student's *t* test results showed that salicylate significantly decreased ($p < 0.05$) the area per headgroup irrespective of NaCl concentration with significant dose dependence in the presence of NaCl.

The effect of salicylate on lipid volumes was also determined by calculating per-lipid volumes. The volume of the lipid bilayer was calculated by multiplying the

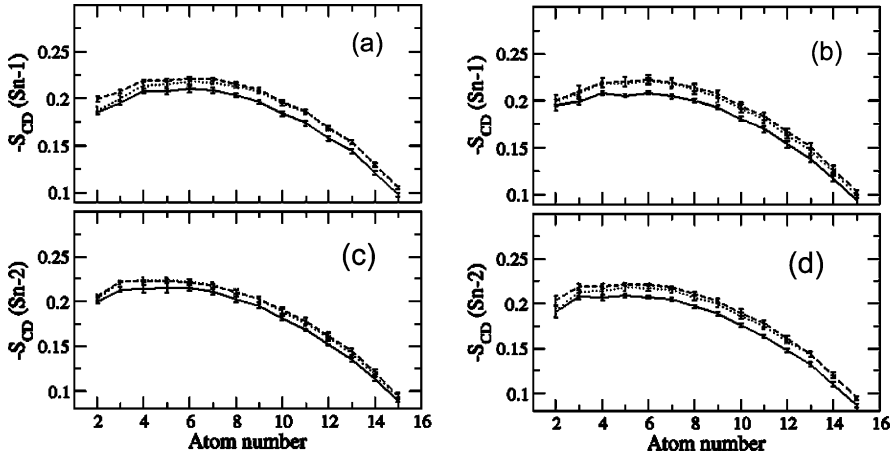

FIGURE 3: Salicylate effects on the order parameters of DPPC acyl chains for (a) $n - 1$ order parameters without NaCl, (b) $n - 1$ order parameters with 150 mM NaCl, (c) $n - 2$ order parameters without NaCl, and (d) $n - 2$ order parameters with 150 mM NaCl. The different lines denote 0 (—), 10 (···), and 60 mM SAL (- - -). Error bars were calculated as described in the text.

projected bilayer surface area by the average bilayer height as determined by the average lipid phosphorus position (*52*, *64*). The per-lipid volume was then obtained by dividing the bilayer volume by the number of lipids. Using this definition, the average volumes per lipid were calculated for the six systems and shown in Figure 2b with error bars obtained by the 5 ns block averaging scheme described above. The simulations produced a volume per lipid for pure DPPC of 1.201 ± 0.001 nm^3, a value that is in good agreement with the experimental result of 1.23 nm^3 (*64*). The presence of salicylate leads to a small reduction in per-lipid volume; however, this reduction is only significant in the absence of NaCl. Additionally, this effect does not change systematically or significantly with salicylate concentration.

Tail Order. The lipid tail order parameter is a standard quantity used to evaluate the structural ordering of acyl chains in a lipid bilayer. In experiments, deuterium order parameters for each CH_2 (CD_2) group can be determined by nuclear magnetic resonance as (*65*)

$$S_{\alpha\beta} = \frac{1}{2}(3\langle \cos\theta_\alpha \cos\theta_\beta \rangle - 1) \quad \alpha, \beta = x, y, z \qquad (1)$$

where θ_α is the angle between the ith molecular axis and the bilayer normal (z axis). The z axis is the molecular axis per CH_2 unit, and x and y axes are assigned on the basis of a right-handed coordinate system. In MD simulations with united atom representations for the CH_2 and CH_3 hydrocarbon groups, the deuterium order parameter can be determined from (*65*)

$$-S_{CD} = \frac{2}{3}S_{xx} + \frac{1}{3}S_{yy} \qquad (2)$$

where S_{xx} and S_{yy} are the order parameters determined with eq 1 by the angle between the axis determined by the $(i - 1)$th, ith, and $(i + 1)$th carbon atoms of the lipid tail and the $x-y$ vector. These definitions provide interpretations for acyl chain order parameters in a bilayer: order parameters assume a maximum value of 1 when the relevant segments are uniformly aligned along the bilayer normal; the order parameters are at a minimum value of -0.5 when the segments are uniformly aligned in the bilayer plane.

The effects of salicylate on lipid tail order parameters are shown in Figure 3 for the cases with and without added NaCl. The Student's t test (*66*) with 95% confidence was used to compare whether the changes of tail order caused by salicylate were significant. For each carbon atom, the mean of the tail order was obtained by averaging the trajectory, and the deviation was calculated from 5 ns block averages of the data, which was similar to the block averaging method presented by Flyvbjerg et al. (*67*). The average simulated tail order parameters in the "plateau" region (carbons 4−8; see Figure 3) of the acyl chain for the pure DPPC bilayer were measured to be -0.208 ± 0.002. This value is in good agreement with experimental measurements of -0.20 ± 0.02 for the same system (*53*). Application of the Student's t test showed that salicylate significantly increased the tail order for systems with 150 mM NaCl and without NaCl ($p < 0.05$); however, the change of the tail order between different concentrations of salicylate was not significant (i.e., no dose dependence). This increase in lipid tail order upon salicylate association is similar to the effect of cholesterol (*34*) but differs from the disordering effects (on some regions of the lipid acyl chain) of molecules such as halothane (*68*).

These changes, together with the area and volume values presented above, suggest that salicylate causes packing and ordering of the bilayer. The possible mechanisms for these phenomena are discussed in the context of salicylate interaction with the DPPC lipids in the following section.

Interaction of Salicylate with Lipid Bilayers. Figure 4 illustrates the orientation of salicylate in the DPPC bilayer for the DPPC/60 mM SAL/NaCl system; similar plots for the other systems with salicylate are provided in Figure 5 of the Supporting Information. The most probable location of salicylate for all four SAL-containing simulations was at the water−bilayer interface, 2−3 nm from the lipid bilayer center. The most probable orientation at the interface was nearly perpendicular with ~30° between the salicylate Z_1 axis (see Figure 4a) and the membrane normal.

To further examine the interaction of the salicylate with the headgroup components of the lipid bilayer, radial distribution functions (RDFs) between the salicylate hydrophilic group (defined below) and components of the lipid headgroup were calculated and are shown in Figure 5a for the DPPC/60 mM SAL/NaCl system. Using the atom naming

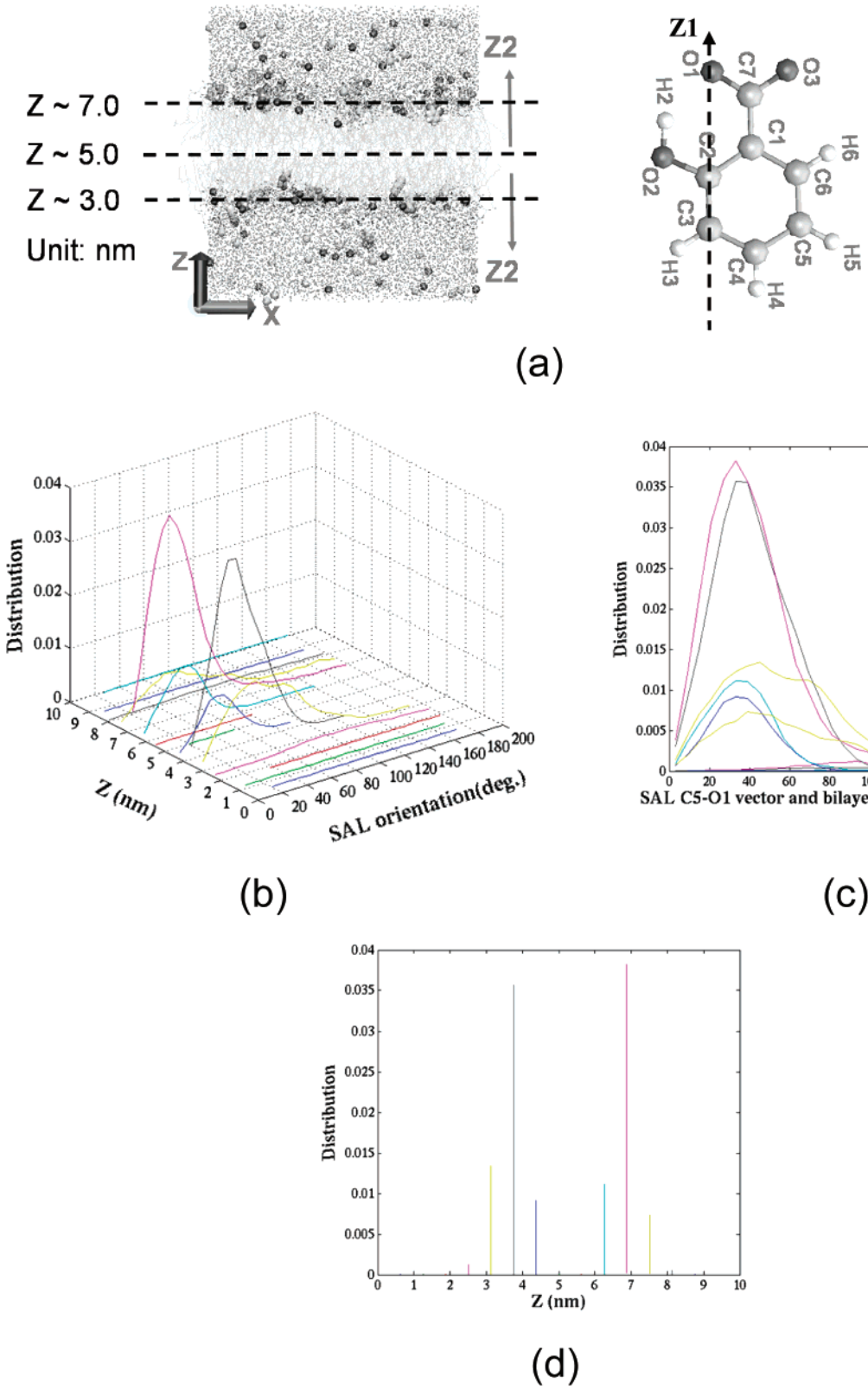

FIGURE 4: Salicylate (SAL) orientation and position distribution within the simulated system (DPPC/60 mM SAL/NaCl system). (a) Salicylate orientation is defined as the angle between the C3−O1 connection of salicylate (Z_1 axis) and the bilayer outward normal (Z_2 axis). (b) Three-dimensional representation of the salicylate orientation and position distribution. (c) Two-dimensional representation of the salicylate orientation distribution. (d) Two-dimensional representation of the salicylate position distribution.

scheme shown in Figure 1, the salicylate hydrophilic group was defined as atoms O1, O2, H2, O3, and C7; the hydrophobic group was defined as atoms C1−C3, H3, C4, H4, C5, H5, C6, and H6. The plots in Figure 5a show the RDFs for the DPPC nitrogen, phosphate, phosphate oxygen, and carbonyl oxygen around the center of salicylate hydrophilic group (defined above). These RDFs illustrate the nature of salicylate coordination by the DPPC headgroups. A snapshot from the MD simulation depicting this coordination between salicylate and lipid is shown in Figure 5b. Plots

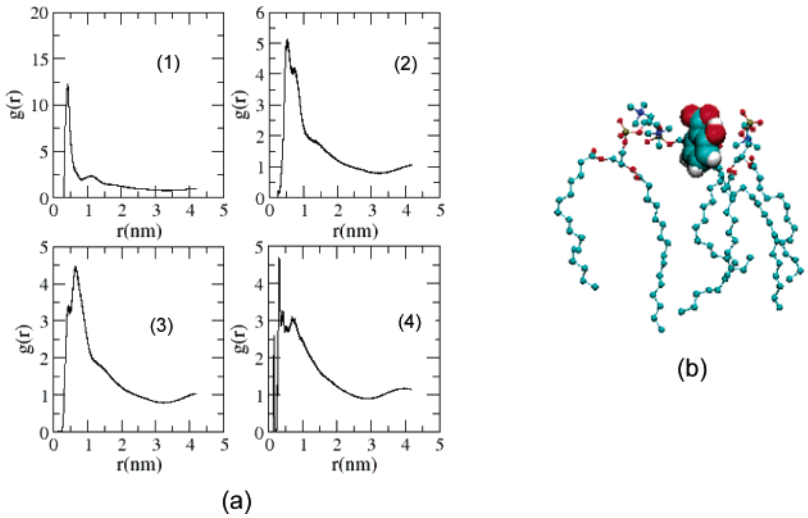

FIGURE 5: Coordination of salicylate by the DPPC lipids for the DPPC/60 mM SAL/NaCl system (plots for the other systems are provided as Supporting Information). (a) Radial distribution functions with respect to the salicylate hydrophilic group for various DPPC components, including the choline nitrogen (1), the phosphate phosphorus (2), the phosphate oxygen (3), and the carbonyl oxygen (4). (b) A snapshot of the MD trajectory showing the salicylate−lipid coordination.

similar to Figure 5a for the other salicylate-containing simulations are provided in Figure 6 of the Supporting Information.

The perpendicular insertion of salicylate into the DPPC bilayer and the tight coordination of salicylate by the DPPC headgroups provide a mechanism for explaining the reduction in surface area observed in the salicylate-containing simulations. In particular, the nearly perpendicular insertion of the salicylate permits tight packing of lipids around the salicylate, while coordination by the DPPC headgroups draws neighboring lipids closer to the salicylate molecule. This mechanism predicts the ordering of lipids as demonstrated by the tail order parameters discussed above. A similar conclusion for reduction of lipid hydrophilic headgroup area by hydroxybenzoic acids was reached by Lin and co-workers (*69*) on the basis of experimental observations of structural transitions in micelles. However, work by Zhou and Raphael on SOPC vesicles under tension demonstrates an *increase* in surface area upon application of salicylate (*16*). More differences between the current study and the work by Zhou and Raphael are discussed in Mechanical Properties.

Effect of Salicylate on Ion Distributions. The binding of salicylate to the DPPC bilayer has a dramatic effect on co- and counterion distributions in the system. Figure 6 depicts the symmetrized distribution of Na^+ and Cl^- ions along the bilayer normal direction. Figure 6a depicts a small, statistically insignificant increase in Na^+ concentrations at the water−lipid interface for all salicylate concentrations. Figure 6b shows that the addition of 10 mM salicylate to the DPPC system did not affect the distribution of Cl^- in the system; however, the addition of 60 mM salicylate significantly reduced ($p < 0.05$) the local concentration of Cl^- at the bilayer−water interface. This change in chloride distribution is likely the result of two factors: the competition of salicylate with Cl^- for coordination by the lipid headgroups (*70*) and the electrostatic repulsion of Cl^- by the salicylate negative charge. This "competition" between chloride and salicylate in the molecular dynamics simulations is indirectly supported by experimental studies which demonstrated a linkage between chloride concentration and the distribution of salicylate across the erythrocyte membranes (*71*). Competition between salicylate and chloride has also been directly observed in OHC studies by Oliver et al. (*21*). While the effect in the OHC also involves interactions with the protein prestin, it indirectly supports our observation of salicylate competition with chloride in biomolecular binding.

Panels e and f of Figure 6 show the relative distribution of salicylate, Na^+, and Cl^- in the DPPC/10 mM SAL/NaCl and DPPC/60 mM SAL/NaCl systems, respectively. The results demonstrate that salicylate penetrates more deeply into the bilayer interior than either Na^+ or Cl^-, especially for higher concentrations of salicylate (60 mM). Given the amphiphilic nature of salicylate, this behavior is not surprising and is consistent with the DPPC coordination of salicylate discussed above. While the location of salicylate is predominantly influenced by its amphiphilic character, the deeper penetration of salicylate into the membrane bilayer may also be related to its larger size and potentially smaller (de)solvation energy, as suggested by studies of Hofmeister-like ion effects in lipid bilayers (*30*).

Electrostatic Potential and Dielectric Properties. The electrostatic potentials of the simulated systems were calculated along the bilayer normal (z). First, mean charge densities for $x-y$ slices of the periodic box were obtained by averaging over the dynamics trajectories. Electrostatic potentials were then calculated from these average charge densities by solving Poisson's equation via an integral of the charge density along the z direction:

$$\varphi(z) - \varphi(z_{\min}) = -\frac{1}{\epsilon_0}\int_{z_{\min}}^{z} dz' \int_{z_{\min}}^{z''} \rho(z'')\, dz'' \qquad (3)$$

where $z_{\min}$ corresponds to the edge of the simulation box, ϵ_0 is the vacuum permeability, and ρ is the charge density along the z direction. The electrostatic potentials of the simulated systems were obtained from the MD trajectory and symmetrized by averaging over the two leaflets of the membrane; the results are shown in panels a and b of Figure 7 with error bars obtained by the block averaging scheme described above. Student's t test values were calculated for three different comparisons for the systems with (Figure 7d) and without (Figure 7c) added NaCl: the 10 mM SAL systems

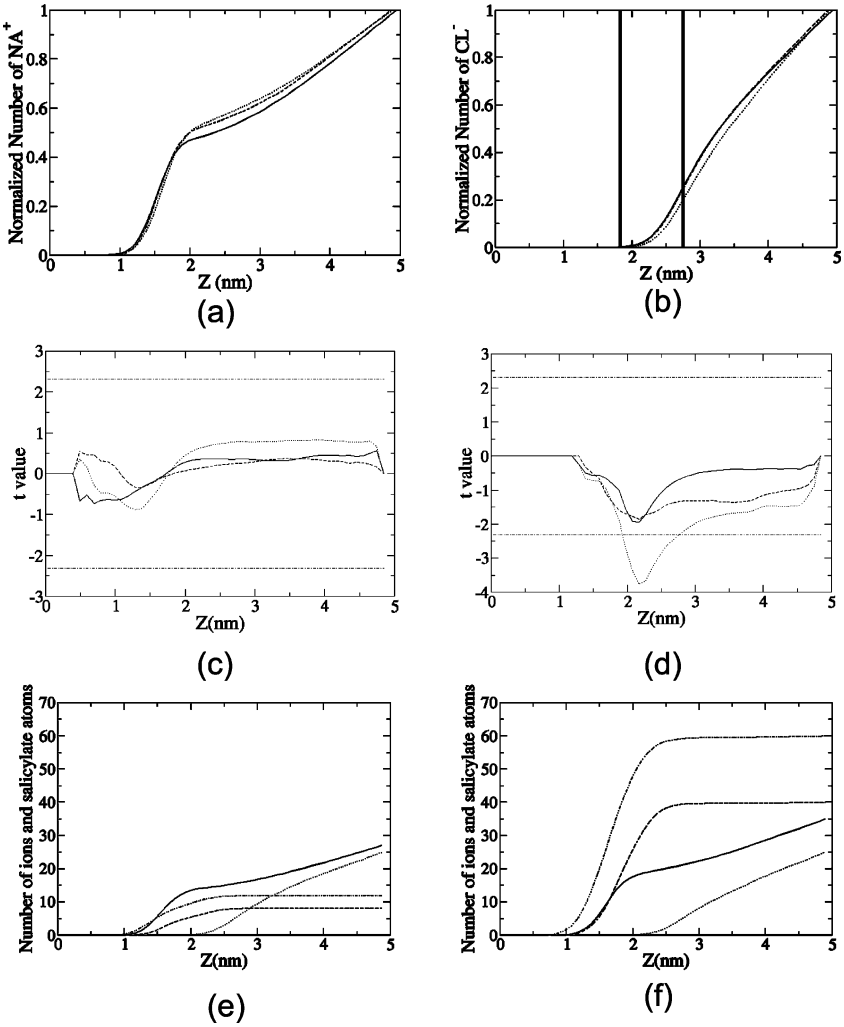

FIGURE 6: Distribution of ions and salicylate atoms between the lipid bilayer center as a function of the position along the lipid bilayer normal direction. For reference, the membrane−water interface lies between 2 and 3 nm (*z*). The top two panels show normalized cumulative number densities for (a) Na^+ for the three NaCl-containing simulations and (b) Cl^- for the three NaCl-containing simulations. In panels a and b, the lines represent different salicylate concentrations: 0 (—), 10 (- - -), and 60 mM SAL (···). The middle panels show Student's *t* values for the number distributions of (c) Na^+ and (d) Cl^- with 10 mM SAL with respect to 0 mM SAL (—), 60 mM SAL with respect to 0 mM SAL (···), and 60 mM SAL with respect to 10 mM SAL (- - -). *t* values corresponding to 5% probability are shown as dotted−dashed lines. The quantities for the number densities were averaged over both leaflets of the bilayer, and error bars were calculated as described in the text. Salicylate significantly decreased ($p < 0.05$) the Cl^- concentrations in the region between the two solid vertical bars. Finally, the bottom panels show the raw cumulative number densities for Na^+ (—), Cl^- (···), SAL hydrophilic group (- - -), and SAL hydrophobic (-·-) from the (e) 10 mM SAL and (f) 60 mM SAL simulations.

with respect to the 0 mM SAL systems, the 60 mM SAL systems with respect to the 0 mM SAL systems, and the 60 mM SAL systems with respect to the 10 mM SAL systems; the resulting *t* values are plotted in panels c and d of Figure 7. These results show that salicylate significantly increased ($p < 0.05$) the electrostatic potential at the water−lipid interface for the simulations without NaCl, but this effect did not show a significant dependence on salicylate concentration. For the simulated systems with NaCl, only 60 mM salicylate caused a significant increase ($p < 0.05$) in the electrostatic potential at the water−lipid interface. This increase is in qualitative agreement with experiments demonstrating salicylate-induced changes in membrane potentials (*17*, *72*) and surface charges (*15*) for human embryonic kidney (HEK) cells as well as various types of neurons (*73*−*76*).

Changes in electrostatic potential can occur for a number of reasons, including variations in local concentrations of counterions (as demonstrated above) or through alteration of the dielectric response properties of the system. The dielectric response of the system is related to the dipole fluctuations through linear response theory (*77*). Previous work by Lin et al. (*78*) as well as more recent theoretical models by Ballenegger and Hansen (*77*) has shown that the dielectric influence of a membranelike inclusion in water extends several hydration layers beyond the water−membrane interface. Therefore, we calculated dielectric coefficients for the entire system as a function of position along the membrane normal. In particular, local dipole moment fluctuation tensors $\mathbf{\Gamma}$ were calculated according to

$$\mathbf{\Gamma}_{\alpha\beta} = \langle M_\alpha M_\beta \rangle - \langle M_\alpha \rangle \langle M_\beta \rangle \quad \alpha, \beta = x, y, z \qquad (4)$$

via decimation of the simulation box into a series of 2.5 Å cubic cells. Dipole moment fluctuation tensors were calculated for each cell, and these results were integrated over the *x* and *y* directions to provide values along the membrane normal. Mean $\mathbf{\Gamma}$ values were obtained by averaging over the

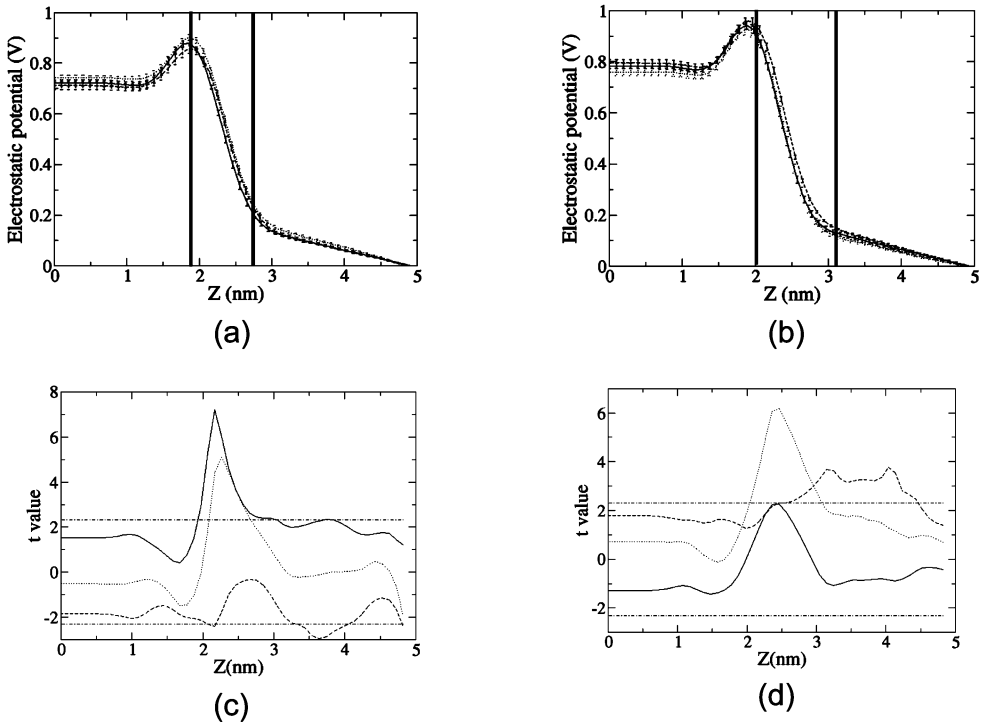

FIGURE 7: Changes in the electrostatic potential due to salicylate. The top two panels show the electrostatic potential profile for the simulations (a) without added NaCl and (b) with 150 mM NaCl for 0 (—), 10 (···), and 60 mM SAL (- - -). The bottom panels show Student's *t* values for the electrostatic potential of the simulations (c) without added NaCl and (d) with 150 mM NaCl for 10 mM SAL with respect to 0 mM SAL (—), 60 mM SAL with respect to 0 mM SAL (···), and 60 mM SAL with respect to 10 mM SAL (- - -). *t* values corresponding to 5% probability are shown as dotted−dashed lines. The quantities for the electrostatic potential were averaged over both leaflets of the bilayer, and error bars were calculated as described in the text. Salicylate significantly increased ($p < 0.05$) the electrostatic potential in the regions between the two solid vertical bars.

MD trajectory; variances were calculated using the 5 ns block averaging method described above. The results of this analysis are shown in Figure 8 and indicate that salicylate significantly affected ($p < 0.05$) dipole moment fluctuations in the system in a dose-independent manner. In particular, salicylate increased dipole moment fluctuations in the solvent region near the water−lipid interface ($z = 2-3$ nm) and decreased dipole moment fluctuation in the lipid bilayer region near the water−lipid interface ($z = 3-4$ nm).

From these analyses, we can conclude that salicylate influences the electrical properties of the membrane system in at least two ways. First, it shifts the distribution of ions at the membrane interface and thereby changes the charge density near the water−bilayer interface. Second, salicylate interacts with the lipid bilayer, bound waters, and ions at the water−lipid interface and thereby reduces the dielectric response of portions of the lipid membrane and increases the response of interfacial water. Both of these changes are likely to be important in the perturbation of cell electrical behavior by salicylate.

Mechanical Properties. Cell membrane mechanical properties are known to play important roles in cellular function through their permeability and deformability. For example, previous studies have shown that the elastic properties of a lipid bilayer influence the function of membrane-bound proteins (*79*). Given the importance of mechanics in outer hair cell function, quantifying the effect of salicylate on bilayer elastic properties is a necessary step in understanding the mechanism of its effect on hearing.

Undulation and Bending Modulus. Small molecule binding is known to influence the undulation and bending mechanics of lipid bilayers (*34*, *80*). A quantitative analysis of the undulation of a lipid bilayer was performed for the six simulated systems using the spectral methods of Lindahl and Edholm (*27*). Membrane undulation was described via a height variable $h(x,y)$ for each lipid defined by the position of the first phospholipid glycol carbon (i.e., the carbon connecting the tails to the headgroup). The choice of the glycol carbon for the height definition differs from the volume calculations carried out above (using the phosphorus); this choice was made for the purposes of comparison with the results of Lindahl and Edholm (*27*). Height variables for each leaflet of the bilayer were mapped to two-dimensional grids with 5 Å spacing in each direction using 2 ps frequency snapshots from the MD trajectory. A two-dimensional Fourier transform of the height grids was calculated according to

$$u(m,n) = \frac{\Delta x \Delta y}{L_x L_y} \sum_{x=0}^{L_X} \sum_{y=0}^{L_Y} h(x,y) \mathrm{e}^{-2\pi i(mx/L_x + ny/L_y)} \qquad (5)$$

where $m = 0, ..., M$, $n = 0, ..., N$, and the wavenumber limits are related to the Nyquist frequency, $M,N = {}^1/_2 f_{\mathrm{Nyquist}}$. The undulation mode spectrum $u(q)$ was calculated by averaging over the two leaflets and reducing the two-dimensional transformed height function to a one-dimensional spectrum over the magnitude of the wave vector:

$$q = |q| = 2\pi \sqrt{\left(\frac{m}{L_x}\right)^2 + \left(\frac{n}{L_y}\right)^2} \qquad (6)$$

Since the area of the simulated lipid bilayer in this study is

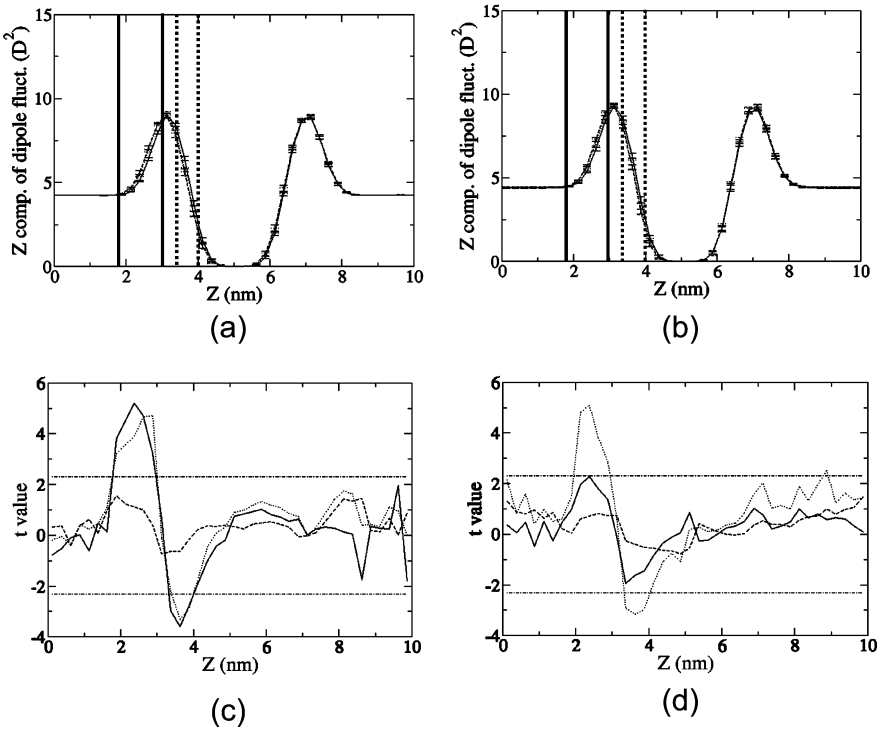

FIGURE 8: Changes in the bilayer normal component of dipole moment fluctuation tensors (Γ_z) for the simulated system. Since salicylate was distributed unevenly across the two leaflets of the lipid bilayer during the MD simulations, the dipole moment fluctuation results were not averaged over the two leaflets. The top two panels show the dipole moment fluctuation tensor Γ_z component for (a) the simulated systems without added NaCl and (b) the simulated systems with 150 mM NaCl for 0 (—), 10 (···), and 60 mM SAL (- - -). The bottom panels show Student's *t* values for the fluctuation tensor normal component of (c) the simulated systems without added NaCl and (d) the simulated systems with 150 mM NaCl for 10 mM SAL with respect to 0 mM SAL (—), 60 mM SAL with respect to 0 mM SAL (···), and 60 mM SAL with respect to 10 mM SAL (- - -). *t* values corresponding to 5% probability are shown as dotted−dashed lines. The error bars were calculated as described in the text. Salicylate significantly increased ($p < 0.05$) dipole moment fluctuation in the regions between the two solid vertical bars and significantly decreased ($p < 0.05$) dipole moment fluctuation in the regions between the two dashed vertical bars.

significantly larger than the membrane thickness, the membrane mechanics can be modeled by an elastic sheet via the relationship (*27*)

$$\langle u^2(q)\rangle = \frac{1}{\beta A_{\text{box}}} \frac{1}{K_{\text{bend}} q^4 + \gamma q^2} \tag{7}$$

where β [$=(k_B T)^{-1}$] is the inverse thermal energy, A_{box} is the projected area of the periodic box, K_{bend} is the bending modulus, γ is the surface tension, q is the wavenumber, and u is the q-space mode magnitude. Since the MD simulations in this study were performed under constant pressure conditions, the surface tension was taken as zero (*24*) and eq 7 was rewritten as

$$\log\langle u^2(q)\rangle = -\log(\beta A_{\text{box}} K_{\text{bend}}) - 4\log(q) \tag{8}$$

This relationship was verified by linear regression of the logarithm of the spectral intensity per mode and the logarithm of the wavenumber (see Table 3). These results indicate that the undulation spectrum scales roughly as expected to $u \sim q^{-4}$ (*27*, *81*) and is independent of salicylate concentration. While the overall undulation spectrum is independent of salicylate concentration, Figure 9 shows some qualitative examples of local changes in membrane structure and curvature due to introduction of salicylate. These changes are further illustrated in the MD trajectory movies provided as Supporting Information. Such perturbation is in qualitative agreement with experimental studies showing that the interaction of the related amphiphile aspirin with membranes induces local conformational changes (*82*, *83*).

Table 3: Results of Linear Regression of the Logarithm of Spectral Intensity per Mode and the Logarithm of the Wavenumber per Eq 10

system	slope	intercept	Pearson correlation coefficient
pure DPPC	3.47 ± 0.05	-2.76 ± 0.03	−0.99
DPPC/10 mM SAL	3.50 ± 0.05	-2.72 ± 0.03	−0.99
DPPC/60 mM SAL	3.57 ± 0.05	-2.67 ± 0.03	−0.99
DPPC/NaCl	3.45 ± 0.06	-2.79 ± 0.04	−0.98
DPPC/10 mM SAL/NaCl	3.50 ± 0.06	-2.77 ± 0.04	−0.99
DPPC/60 mM SAL/NaCl	3.47 ± 0.06	-2.77 ± 0.04	−0.99

Although the bending modulus can be determined from eq 8, we chose to calculate the bending modulus for each system from the total root-mean-square (rms) amplitude of the undulation modes in the system (*27*)

$$\langle u^2\rangle \approx \frac{A_{\text{box}}}{257\beta K_{\text{bend}}} \tag{9}$$

where u is the undulation intensity in Fourier space. Bending moduli for each of the MD systems were calculated via eq 9 with means and deviations obtained using the 5 ns block averaging scheme described above. The pure DPPC system gave a bending modulus of $(10 \pm 3) \times 10^{-20}$ J, a value in reasonable agreement with the experimental result of 5.5 ×

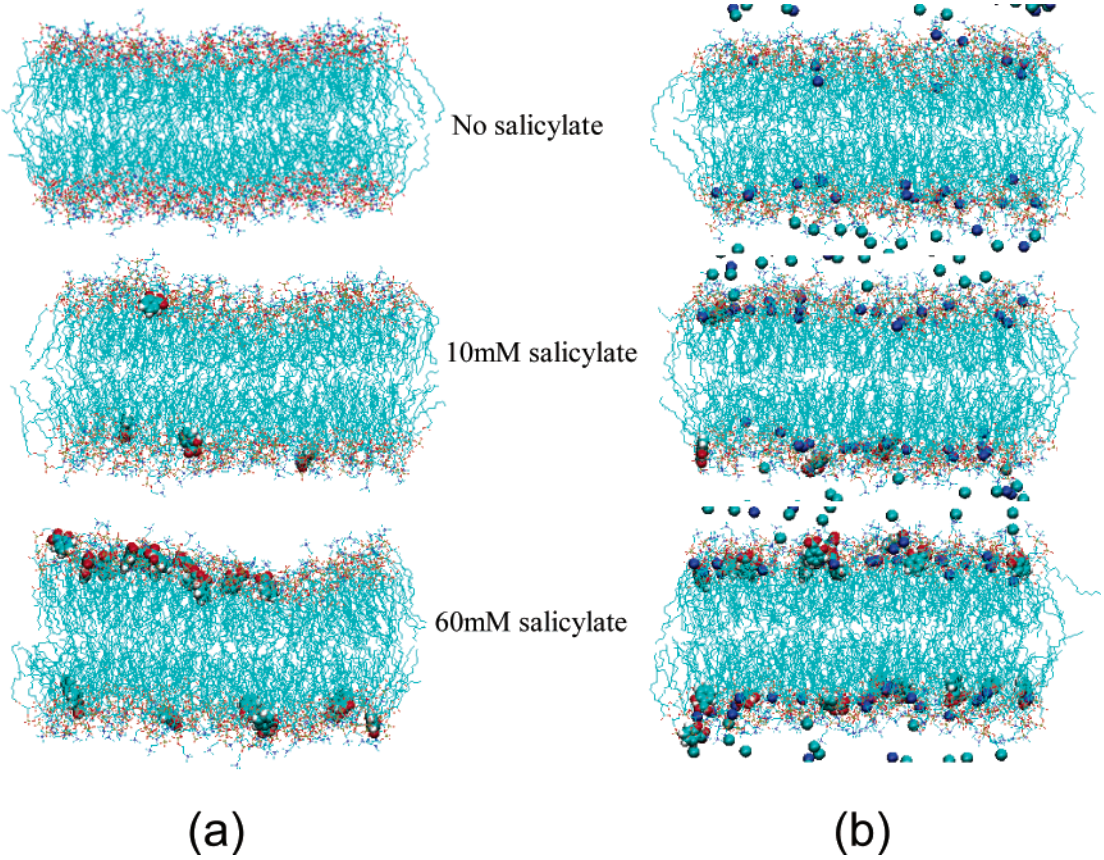

FIGURE 9: Snapshots from the MD simulations (a) without NaCl and (b) with 150 mM NaCl for (top) systems without salicylate, (middle) systems with 10 mM salicylate, and (bottom) systems with 60 mM salicylate. Complete movies for these trajectories are available as Supporting Information.

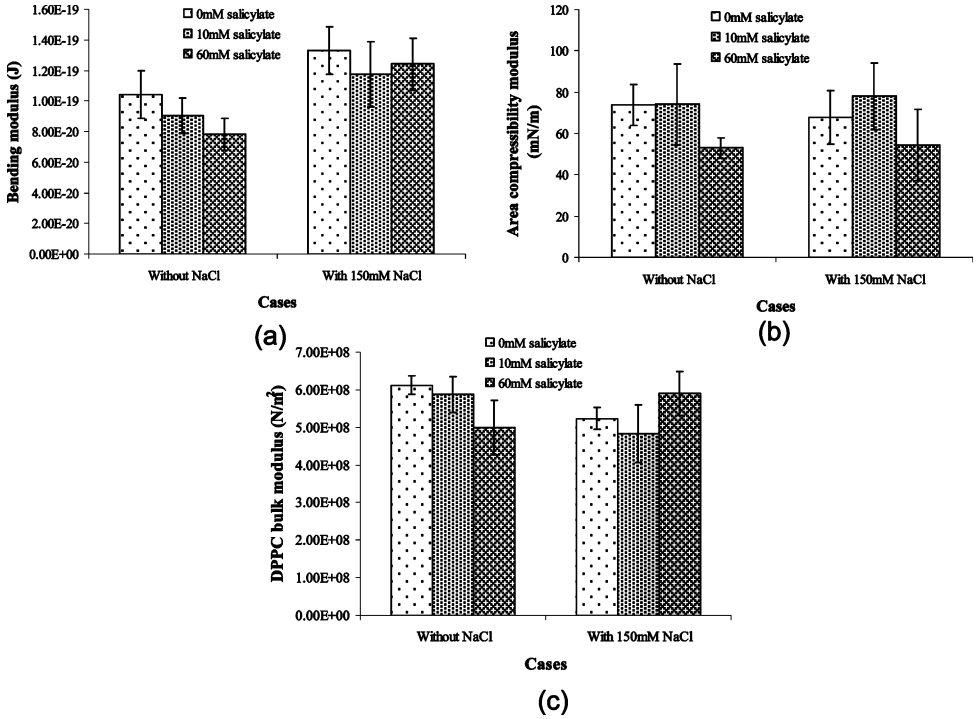

FIGURE 10: Mechanical properties of the lipid bilayer with error bars were calculated as described in the text: (a) bending modulus, (b) area compressibility modulus, and (c) bulk modulus. There were no significant differences in the simulated systems.

10^{-20} J (*84*). The results of these analyses are shown in Figure 10a and indicate that salicylate decreases the bending modulus of the bilayer in a small, statistically insignificant ($p < 0.05$) manner. These results are different than the experimental results of Zhou and Raphael (*16*), who showed that application of salicylate resulted in a significant decrease in the bending modulus of stearoyloleoylphosphatidylcholine (SOPC) giant unilamellar vesicles (GUVs) under tension. While the simulations described here could contain artifacts from finite domain sizes and finite sampling, differences with

the Zhou and Raphael experiments could also be due to different lipid types (SOPC) and different surface tensions. Interestingly, our results do agree with several experiments on larger-scale systems which show no effect of salicylate on mechanical properties. In particular, membrane tether experiments (*85*) demonstrated that salicylate does not significantly affect the membrane mechanics of OHC lateral walls (*13*, *14*, *86*) or HEK cell membranes (*14*, *86*). Our observations are also in agreement with atomic force microscopy experiments of Zhang et al. which observed a salicylate-induced change in the HEK membrane surface charge but no change in membrane mechanics (force−displacement profiles) (*15*). Similarly, the work of Hallworth (*8*) showed that salicylate changes the force generation of OHCs without a change in OHC stiffness. Finally, Morimoto et al. demonstrated that salicylate did not change the pressure required for vesiculation of OHC lateral walls (*9*). Unlike the SOPC work of Zhou and Raphael, these are experiments on cells and therefore differ in that they contain a number of additional components (cytoskeleton, membrane proteins, etc.) not included in the simulations presented here; however, they do provide qualitative support for our observations.

Area Compressibility Modulus. Area compressibility moduli describe the energetics of increases and decreases in membrane areas. These moduli have previously been calculated from either surface tensions (*24*), fluctuations in projected membrane area (*24*, *34*), or fluctuations in area per lipid (*24*). Since the MD simulations in this study were performed under isotropic constant pressure, fluctuations in membrane area were used to calculate the area compressibility moduli. However, to account for the contribution of bound ions and salicylate to the membrane area, we employed the total membrane solvent-accessible surface area (SASA) rather than the total projected membrane area used in other MD analyses (*24*, *34*). The SASA was calculated using a waterlike spherical probe of 1.4 Å with GROMACS version 3.2.1. We then determined the area compressibility moduli of the simulated systems from the fluctuations in the SASA according to the usual formula (*24*)

$$K_{\text{area}} = \frac{A}{\beta \sigma_A^{\,2}} \tag{10}$$

where K_{area} is the area compressibility modulus, A is the SASA, and σ_A is the fluctuation of the SASA. Means and averages for the moduli were determined from the trajectory using the block averaging scheme described above. The pure DPPC simulation gave a compressibility modulus of 70 ± 20 mN m^{-1}, a value which underestimates the experimental result of 250 mN m^{-1} (*64*, *87*). Differences between this value and experiment could be caused by a number of reasons, including finite size and sampling effects (*24*) and the specific pressure regulation method used for this simulation. The results for the six systems are presented in Figure 10b and demonstrate that salicylate did not significantly decrease the area compressibility modulus of the DPPC bilayer.

As with the bending moduli reported above, these results are different from those of the SOPC GUV experiments of Zhou and Raphael (*16*) but agree with studies of the salicylate effect on cellular mechanics (*8*, *9*, *13*−*15*, *86*).

Bulk Modulus. The bulk modulus measures the volume compressibility of the system. For our constant pressure simulations, the bulk moduli were calculated from the fluctuations of the volume of the system according to (*88*)

$$K_{\text{bulk}} = \frac{V}{\beta \sigma_V^{\,2}} \tag{11}$$

where K_{bulk} is the bulk modulus, V is the volume of the lipid bilayer, and σ_V is the fluctuation of the volume of the lipid bilayer. The volume of the lipid bilayer was calculated using the lipid phosphorus position in the same manner as the per-lipid volume calculations described above. Bulk modulus means and deviations were determined by the 5 ns block averaging method described above. The lipid bilayer bulk moduli for the six simulated systems are plotted in Figure 10c; the results show that salicylate did not significantly affect the bulk modulus.

Bulk moduli were not available from the SOPC GUV experiments of Zhou and Raphael (*16*); however, our results do agree with studies of salicylate effects on cell mechanics (*8*, *9*, *13*−*15*, *86*). However, our calculated bulk modulus for the pure DPPC lipid bilayer at a temperature of 323 K was (6.1 ± 0.3) × 10^8 N m^{-2}. Like the area compressibility modulus, this value differs from the experimental measurements of 2.2 × 10^9 N m^{-2} for DPPC (*89*). Possible reasons for this difference were discussed above and include the usual potential finite size and sampling artifacts associated with MD simulations (*24*).

CONCLUSIONS

The effect of salicylate on the microscopic and mesoscopic properties of a DPPC lipid bilayer was investigated with molecular dynamics simulations. Results from this study showed that salicylate significantly affected a number of bilayer structural properties, including a reduction in the membrane area and increased ordering of the lipid acyl tails. These changes were interpreted in terms of the tight coordination of salicylate by the DPPC headgroups and the nearly perpendicular orientation of salicylate in the bilayer which permitted tight membrane packing, a mechanism which is supported by studies of salicylate-induced structural changes in micelles (*69*). Salicylate introduced a local increase in the level of Na^+ and a decrease in the level of Cl^- near the bilayer−water interface. This competition between salicylate and chloride was qualitatively supported by similar observations in OHCs (*21*). The binding of this amphiphile also changed the electrostatic potential and dielectric response of the system, with significant changes near the membrane−water interface. These results were shown to be in qualitative agreement with a number of experimental observations, including salicylate-induced changes in membrane electrostatic potentials (*17*, *72*) and surface charges (*15*). Finally, we observed no changes in the mechanical properties of the system due to salicylate binding. This lack of change was discussed in light of experimental evidence (on somewhat different membrane systems) which supported (*8*, *9*, *13*, *15*, *86*) and contradicted (*16*) our observations. Interestingly, most of the salicylate effects described above were independent of dosage, an observation which is in reasonable agreement with the results of Kakehata

et al., who found that the OHC response to salicylate was saturated at ~10 mM (*19*).

As mentioned in the introductory section, the ultimate goal of this research was to help understand the hearing-related side effects of salicylate in the context of OHC membrane electrical and mechanical properties. There is clearly a significant gap between the existing DPPC model bilayer and the complexity of the OHC and its biological surroundings. Fortunately, there are a number of recent computational developments, including methods for simulating asymmetric electrolyte solutions and potential gradients around lipid bilayers (*90*) and coarse-grained simulations of large biomembranes (*28*, *29*), which will allow us to pursue more realistic models of amphiphile effects on OHC hearing in the future. Therefore, present models provide important insight into salicylate interaction with model membranes and the basis for future multiscale research into understanding the macroscopic effects of ligand-induced changes in membrane properties.

ACKNOWLEDGMENT

Y.S. thanks M. Bradley and T. Dolinsky for helpful discussions. N.A.B. and Y.S. thank Dr. W. E. Brownell for the initial suggestion of this project and continuing insightful discussions, Drs. B. Farrell and R. M. Raphael for numerous helpful suggestions on the project and the manuscript, M. Kaneda for her preliminary work on this project, and M. Bradley and A. Vitalis for critical reading of the manuscript.

SUPPORTING INFORMATION AVAILABLE

Additional data, including figures of the QM/MM setup, time courses for system area, volume, and potential energy, selected membrane dynamical properties, additional data for Figures 4 and 5, and movies of the molecular dynamics simulations. This material is available free of charge via the Internet at http://pubs.acs.org.

REFERENCES

1. Roberts, L. J., II, and Morrow, J. D. (2001) Analgesic-antipyretic and antiinflammatory agents and drugs employed in the treament of gout, in *The Pharmacological Basis of Therapeutics* (Hardman, J. G., Limbird, L. E., and Goodman Gilman, A., Eds.) McGraw-Hill Medical Publishing Division, Chicago.
2. Shehata, W. E., Brownell, W. E., and Dieler, R. (1991) Effects of salicylate on shape, electromotility and membrane characteristics of isolated outer hair cells from guinea pig cochlea, *Acta Oto-Laryngol. 111*, 707−18.
3. Myers, E. N., and Bernstein, J. M. (1965) Salicylate ototoxicity: A clinical and experimental study, *Arch. Otolaryngol. 82*, 483−93.
4. Myers, E. N., Bernstein, J. M., and Fostiropolous, G. (1965) Salicylate ototoxicity: A clinical study, *N. Engl. J. Med. 273*, 587−90.
5. Jung, T. T., Rhee, C. K., Lee, C. S., Park, Y. S., and Choi, D. C. (1993) Ototoxicity of salicylate, nonsteroidal antiinflammatory drugs, and quinine, *Otolaryngol. Clin. North Am. 26*, 791−810.
6. Tunstall, M. J., Gale, J. E., and Ashmore, J. F. (1995) Action of salicylate on membrane capacitance of outer hair cells from the guinea-pig cochlea, *J. Physiol. 485*, 739−52.
7. Lue, A. J., and Brownell, W. E. (1999) Salicylate induced changes in outer hair cell lateral wall stiffness, *Hear. Res. 135*, 163−8.
8. Hallworth, R. (1997) Modulation of outer hair cell compliance and force by agents that affect hearing, *Hear. Res. 114*, 204−12.
9. Morimoto, N., Raphael, R. M., Nygren, A., and Brownell, W. E. (2002) Excess plasma membrane and effects of ionic amphipaths on mechanics of outer hair cell lateral wall, *Am. J. Physiol. 282*, C1076−86.
10. Stewart, C. E., and Hudspeth, A. J. (2000) Effects of salicylates and aminoglycosides on spontaneous otoacoustic emissions in the Tokay gecko, *Proc. Natl. Acad. Sci. U.S.A. 97*, 454−9.
11. Grosh, K., Zheng, J., Zou, Y., de Boer, E., and Nuttall, A. L. (2004) High-frequency electromotile responses in the cochlea, *J. Acoust. Soc. Am. 115*, 2178−84.
12. Ashmore, J., and Gale, J. (2004) The cochlear amplifier, *Curr. Biol. 14*, R403−4.
13. Ermilov, S., Brownell, W. E., and Anvari, B. (2004) in *Proceedings of SPIE* (Cartwright, A. N., Ed.) pp 136−42, The International Society for Optical Engineering, Bellingham, WA.
14. Anvari, B., Qian, F., Pereria, F. A., and Brownell, W. E. (2005) Prestin-lacking membranes are capable of high-frequency electromechanical transduction, in *Auditory Mechanisms: Processes and Models* (Nuttall, A. L., Ed.) World Scientific, London (in press).
15. Zhang, P.-C., Keleshian, A. M., and Sachs, F. (2001) Voltage-induced membrane movement, *Nature 413*, 428−32.
16. Zhou, Y., and Raphael, R. M. (2004) Effect of salicylate on the elasticity, bending stiffness, and strength of SOPC membranes, *Biophys. J.* (in press).
17. Farrell, B., Shope, C. D., and Brownell, W. E. (2005) Voltage Dependent Capacitance of Human Embryonic Kidney (HEK) Cells (in review).
18. Mazorow, D. L., Haug, A., Bull, R., and McGroarty, E. J. (1985) Effects of aspirin, indomethacin, and sodium salicylate on human erythrocyte membranes as detected with electron spin resonance spectroscopy, *Thromb. Res. 40*, 779−92.
19. Kakehata, S., and Santos-Sacchi, J. (1996) Effects of salicylate and lanthanides on outer hair cell motility and associated gating charge, *J. Neurosci. 16*, 4881−9.
20. Oghalai, J. S., Zhao, H.-B., Kutz, J. W., and Brownell, W. E. (2000) Voltage- and Tension-Dependent Lipid Mobility in the Outer Hair Cell Plasma Membrane, *Science 287*, 658−61.
21. Oliver, D., He, D. Z., Klocker, N., Ludwig, J., Schulte, U., Waldegger, S., Ruppersberg, J. P., Dallos, P., and Fakler, B. (2001) Intracellular anions as the voltage sensor of prestin, the outer hair cell motor protein, *Science 292*, 2340−3.
22. Dong, X.-X., and Iwasa, K. H. (2004) Tension Sensitivity of Prestin: Comparison with the Membrane Motor in Outer Hair Cells, *Biophys. J. 86*.
23. Song, L., Seeger, A., and Santos-Sacchi, J. (2005) On Membrane Motor Activity and Chloride Flux in the Outer Hair Cell: Lessons Learned from the Environmental Toxin Tributyltin, *Biophys. J. 88*, 2350−62.
24. Feller, S. E., and Pastor, R. W. (1999) Constant surface tension simulations of lipid bilayers: The sensitivity of surface areas and compressibilities, *J. Chem. Phys. 111*, 1281−7.
25. Pandit, S. A., Bostick, D., and Berkowitz, M. L. (2003) Mixed Bilayer Containing Dipalmitoylphosphatidylcholine and Dipalmitoylphosphatidylserine: Lipid Complexation, Ion Binding, and Electrostatics, *Biophys. J. 85*, 3120−31.
26. Tieleman, D. P., and Berendsen, H. J. C. (1996) Molecular dynamics simulations of a fully hydrated dipalmitoylphosphatidylcholine bilayer with different macroscopic boundary conditions and parameters, *J. Chem. Phys. 105*, 4871−80.
27. Lindahl, E., and Edholm, O. (2000) Mesoscopic undulations and thickness fluctuations in lipid bilayers, *Biophys. J. 79*, 426−33.
28. Ayton, G., and Voth, G. A. (2002) Bridging microscopic and mesoscopic simulations of lipid bilayers, *Biophys. J. 83*, 3357−70.
29. Pickholz, M., Saiz, L., and Klein, M. L. (2005) Concentration Effects of Volatile Anesthetics on the Properties of Model Membranes: A Coarse-Grain Approach, *Biophys. J. 88*, 1524−34.
30. Sachs, J. N., and Woolf, T. B. (2003) Understanding the Hofmeister effect in interactions between chaotropic anions and lipid bilayers: Molecular dynamics simulations, *J. Am. Chem. Soc. 125*, 8742−3.
31. Pasenkiewicz-Gierula, M., Róg, T., Grochowski, J., Serda, P., Czarnecki, R., Librowski, R., and Lochyski, S. (2003) Effects of a Carane Derivative Local Anesthetic on a Phospholipid Bilayer Studied by Molecular Dynamics Simulation, *Biophys. J. 85*, 1248−58.
32. Pereira, C. S., Lins, R. D., Chandrasekhar, I., Freitas, L. C. G., and Hünenberger, P. H. (2004) Interaction of the Disaccharide

Trehalose with a Phospholipid Bilayer: A Molecular Dynamics Study, *Biophys. J. 86*, 2273−85.
33. Smondyrev, A. M., and Berkowitz, M. L. (1999) Molecular dynamics simulation of DPPC bilayer in DMSO, *Biophys. J. 76*, 2472−8.
34. Hofsäss, C., Lindahl, E., and Edholm, O. (2003) Molecular Dynamics Simulations of Phospholipid Bilayers with Cholesterol, *Biophys. J. 84*, 2192−206.
35. Villareal, M. A., Díaz, S. B., Disalvo, E. A., and Montich, G. G. (2004) Molecular Dynamics Simulation Study of the Interaction of Trehalose with Lipid Membranes, *Langmuir 20*, 7844−51.
36. Lee, B. W., Faller, R., Sum, A. K., Vattulainen, I., Patra, M., and Karttunen, M. (2004) Structural effects of small molecules on phospholipid bilayers investigated by molecular simulations, *Fluid Phase Equilib. 225*, 63−8.
37. Sum, A. K., Faller, R., and de Pablo, J. J. (2003) Molecular Simulation Study of Phospholipid Bilayers and Insights of the Interactions with Disaccharides, *Biophys. J. 85*, 2830−44.
38. Dickey, A. N., and Faller, R. (2005) Investigating interactions of biomembranes and alcohols: A multiscale approach, *J. Polym. Sci., Part B: Polym. Phys. 43*, 1025−32.
39. Murray, D., and Honig, B. (2002) Electrostatic control of the membrane targeting of C2 domains, *Mol. Cell 9*, 145−54.
40. Diraviyam, K., Stahelin, R. V., Cho, W., and Murray, D. (2003) Computer modeling of the membrane interaction of FYVE domains, *J. Mol. Biol. 328*, 721−36.
41. Lopez, C. F., Nielsen, S. O., Moore, P. B., and Klein, M. L. (2004) Understanding nature's design for a nanosyringe, *Proc. Natl. Acad. Sci. U.S.A. 101*, 4431−4.
42. Zhu, F., Tajkhorshid, E., and Schulten, K. (2004) Theory and Simulation of Water Permeation in Aquaporin-1, *Biophys. J. 86*, 50−7.
43. Lindahl, E., Hess, B., and van der Spoel, D. (2001) GROMACS 3.0: A package for molecular simulation and trajectory analysis, *J. Mol. Model. 7*, 306−17.
44. Kleywegt, G. J., and Jones, T. A. (1998) Databases in protein crystallography, *Acta Crystallogr. D54*, 1119−31.
45. van Aalten, D. M. F., Bywater, R., Findlay, J. B. C., Hendlich, M., Hooft, R. W. W., and Vriend, G. (1996) PRODRG, a program for generating molecular topologies and unique molecular descriptors from coordinates of small molecules, *J. Comput.-Aided Mol. Des. 10*, 255−62.
46. *QSite* (2001) Schrödinger, Inc., New York.
47. Philipp, D. M., and Friesner, R. A. (1999) Mixed ab initio QM/MM modeling using frozen orbitals and tests with alanine dipeptide and tetrapeptide, *J. Comput. Chem. 20*, 1468−94.
48. Murphy, R. B., Philipp, D. M., and Friesner, R. A. (2000) A mixed quantum mechanics/molecular mechanics (QM/MM) method for large-scale modeling of chemistry in protein environments, *J. Comput. Chem. 21*, 1442−57.
49. Kaminski, G., Friesner, R. A., Tirado-Rives, J., and Jorgensen, W. L. (2001) Evaluation and reparametrization of the OPLS-AA force field for proteins via comparison with accurate quantum chemical calculations on peptides, *J. Phys. Chem. B 105*, 6474−87.
50. Ponder, J. W., and Case, D. A. (2003) Force fields for protein simulations, *Adv. Protein Chem. 66*, 27−85.
51. Berger, O., Edholm, O., and Jahnig, F. (1997) Molecular dynamics simulations of a fluid bilayer of dipalmitoylphosphatidylcholine at full hydration, constant pressure, and constant temperature, *Biophys. J. 72*, 2002−13.
52. Nagle, J. F., and Wiener, M. C. (1988) Structure of fully hydrated bilayer dispersions, *Biochim. Biophys. Acta 942*, 1−10.
53. Seelig, A., and Seelig, J. (1974) Dynamic structure of fatty acyl chains in a phospholipid bilayer measured by deuterium magnetic resonance, *Biochemistry 13*, 4839−45.
54. Marrink, S.-J., Berger, O., Tieleman, P., and Jähnig, F. (1998) Adhesion Forces of Lipids in a Phospholipid Membrane Studied by Molecular Dynamics Simulations, *Biophys. J. 74*, 931−43.
55. Berendsen, H. J. C., Grigera, J. R., and Straatsma, T. P. (1987) The missing term in effective pair potentials, *J. Phys. Chem. 91*, 6269−71.
56. Böckmann, R. A., Hac, A., Heimburg, T., and Grubmüller, H. (2003) Effect of Sodium Chloride on a Lipid Bilayer, *Biophys. J. 85*, 1647−55.
57. Nagle, J. F., Zhang, R., Tristram-Nagle, S., Sun, W., Petrache, H. I., and Suter, R. M. (1996) X-ray structure determination of fully hydrated L α phase dipalmitoylphosphatidylcholine bilayers, *Biophys. J. 70*, 1419−31.
58. Parrinello, M., and Rahman, A. (1981) Polymorphic transitions in single crystals: A new molecular dynamics method, *J. Appl. Phys. 52*, 7182−90.
59. Hoover, W. G. (1985) Canonical dynamics: Equilibrium phase-space distributions, *Phys. Rev. A 31*, 1695−7.
60. Darden, T., York, D., and Pedersen, L. G. (1993) Particle mesh Ewald: An N·log(N) method for Ewald sums in large systems, *J. Chem. Phys. 98*, 10089−92.
61. Patra, M., Karttunen, M., Hyvönen, M. T., Falck, E., and Vattulainen, I. (2004) Lipid Bilayers Driven to a Wrong Lane in Molecular Dynamics Simulations by Subtle Changes in Long-Range Electrostatic Interactions, *J. Phys. Chem. B 108*, 4485−94.
62. Patra, M., Karttunen, M., Hyvönen, M. T., Falck, E., Lindqvist, P., and Vattulainen, I. (2003) Molecular Dynamics Simulations of Lipid Bilayers: Major Artifacts Due to Truncating Electrostatic Interactions, *Biophys. J. 84*, 3636−45.
63. Petrache, H. I., Dodd, S. W., and Brown, M. F. (2000) Area per Lipid and Acyl Length Distributions in Fluid Phosphatidylcholines Determined by ^{2}H NMR Spectroscopy, *Biophys. J. 79*, 3172−92.
64. Nagle, J. F., and Tristram-Nagle, S. (2000) Structure of lipid bilayers, *Biochim. Biophys. Acta 1469*, 159−95.
65. Egberts, E., and Berendsen, H. J. C. (1988) Molecular dynamics simulation of a smectic liquid crystal with atomic detail, *J. Chem. Phys. 89*, 3718−32.
66. Bailey, N. T. J. (1995) *Statistical Methods in Biology*, 3rd ed., Cambridge University Press, New York.
67. Flyvbjerg, H., and Petersen, H. G. (1989) Error estimates on averages of correlated data, *J. Chem. Phys. 91*, 461−6.
68. Koubi, L., Tarek, M., Klein, M. L., and Scharf, D. (2000) Distribution of Halothane in a Dipalmitoylphosphatidylcholine Bilayer from Molecular Dynamics Calculations, *Biophys. J. 78*, 800−11.
69. Lin, Z., Cai, J. J., Scriven, L. E., and Davis, H. T. (1994) Spherical-to-Wormlike Micelle Transition in CTAB Solutions, *J. Phys. Chem. 98*, 5984−93.
70. Sachs, J. N., Nanda, H., Petrache, H. I., and Woolf, T. B. (2004) Changes in Phosphatidylcholine Headgroup Tilt and Water Order Induced by Monovalent Salts: Molecular Dynamics Simulations, *Biophys. J. 86*, 3772−82.
71. Nwafor, A., and Coakley, W. T. (1985) Drug-induced shape change in erythrocytes correlates with membrane potential change and is independent of glycocalyx charge, *Biochem. Pharmacol. 34*, 3329−36.
72. McLaughlin, S. (1973) Salicylates and phospholipid bilayer membranes, *Nature 243*, 234−5.
73. Cohen, I., Noble, D., Ohba, M., and Ojeda, C. (1979) Action of salicylate ions on the electrical properties of sheep cardiac Purkinje fibres, *J. Physiol. 297*, 163−85.
74. Levitan, H., and Barker, J. L. (1972) Membrane Permeability: Cation Selectivity Reversibly Altered by Salicylate, *Science 178*, 63−4.
75. Levitan, H., and Barker, J. L. (1972) Salicylate: A Structure−Activity Study of its Effects on Membrane Permeability, *Science 176*, 1423−5.
76. Attwell, D., Bergman, C., and Ojeda, C. (1979) The action of salicylate ions on the frog node of Ranvier, *J. Physiol. 295*, 69−81.
77. Ballenegger, V., and Hansen, J.-P. (2005) Dielectric permittivity profiles of confined polar fluids, *J. Chem. Phys. 122*, 114711.
78. Lin, J.-H., Baker, N. A., and McCammon, J. A. (2002) Bridging the implicit and explicit solvent approaches for membrane electrostatics, *Biophys. J. 83*, 1374−9.
79. Roux, B., and Schulten, K. (2004) Computational Studies of Membrane Channels, *Structure 12*, 1343−51.
80. Ly, H. V., and Longo, M. L. (2004) The Influence of Short-Chain Alcohols on Interfacial Tension, Mechanical Properties, Area/Molecule, and Permeability of Fluid Lipid Bilayers, *Biophys. J. 87*, 1013−33.
81. Goetz, R., Gompper, G., and Lipowsky, R. (1999) Mobility and Elasticity of Self-Assembled Membranes, *Phys. Rev. Lett. 82*, 221−4.
82. Watala, C., and Gwozdzinski, K. (1993) Effect of aspirin on conformation and dynamics of membrane proteins in platelets and erythrocytes, *Biochem. Pharmacol. 45*, 1343−9.

83. Sheetz, M. P., and Singer, S. J. (1976) Equilibrium and kinetic effects of drugs on the shapes of human erythrocytes, *J. Cell Biol. 70*, 247−51.
84. Petrache, H. I., Gouliaev, N., Tristram-Nagle, S., Zhang, R., Suter, R. M., and Nagle, J. F. (1998) Interbilayer interactions from high-resolution X-ray scattering, *Phys. Rev. E 57*, 7014−24.
85. Qian, F., Ermilov, S., Murdock, D., Brownell, W. E., and Anvari, B. (2004) Combining optical tweezers and patch clamp for studies of cell membrane electromechanics, *Rev. Sci. Instrum. 75*, 2937−42.
86. Ermilov, S. A., Murdock, D. R., Brownell, W. E., and Anvari, B. (2005) Effects of salicylate on plasma membrane mechanics, *J. Neurophysiol.* (in press).
87. Rawicz, W., Olbrich, K. C., McIntosh, T., Needham, D., and Evans, E. (2000) Effect of Chain Length and Unsaturation on Elasticity of Lipid Bilayers, *Biophys. J. 79*, 328−39.
88. Hansen, J.-P., and McDonald, I. R. (2000) *Theory of Simple Liquids*, 2nd ed., Academic Press, San Diego.
89. Mitaku, S., Ikegami, A., and Sakanishi, A. (1978) Ultrasonic studies of lipid bilayer. Phase transition in synthetic phosphatidylcholine liposomes, *Biophys. Chem. 8*, 295−304.
90. Sachs, J. N., Crozier, P. S., and Woolf, T. B. (2004) Atomistic simulations of biologically realistic transmembrane potential gradients, *J. Chem. Phys. 121*, 10847−51.

BI0506829